Journal of Theoretical and Applied Information Technology

15th September 2023. Vol.101. No 17

ISSN: 1992-8645 www.jatit.org E-ISSN: 1817-3195

A MULTIFRACTAL APPROACH FOR TEXTURE CLASSIFICATION APPLIED TO THE KIDNEY ULTRASOUND IMAGES

TAHIRI ALAOUI M[1,2], KORCHIYNE R[3],FARSSI S M[4], TOUZANI A[5]

[1] Computer Science, Applied Mathematics, Artificial Intelligence and Pattern Recognition Team, Faculty of Sciences, Mohammed V University, Rabat, Morocco
[2] Hassan II Academy of Sciences and Technology
[3]Computer Research Laboratory, Superior School of Technology, Ibn Tofaïl University, Kenitra, Morocco
[4]Laboratory of medical Images and Bioinformatics, Polytechnic High School, Cheikh Anta Diop University Dakar, Senegal
[5]Laboratoire d'Automatique et Informatique Industrielle, E.M.I. - B.P. 765, Agdal, Rabat, Morocco

E-mail: [1,2] m.alaoui@academiesciences.ma , [3] redouan.korchiyne@uit.ac.ma

ABSTRACT

The realization of diagnostic decision support systems in medical imaging, in particular ultrasound imaging, is a field that continues to experience more and more success thanks to the development of image processing tools allowing segmentation and texture characterization which lead to pattern recognition with a minimum of error. Indeed, concerning the characterization of the texture of ultrasound images, in addition to statistical techniques, several methods based on new approaches are proposed. Indeed, multifractal analysis in texture characterization is becoming increasingly efficient due to multifractal modelling and powerful methods in estimation of irregularities functions and multifractal spectrum. But of all methods proposed for texture characterization, in particular methods using multifractal tools, the extraction of discriminating texture features remains a major challenge.

In this respect, as a first main contribution, we propose a multifractal approach, based on two multifractal descriptions, for texture characterization that we used, in the second main contribution, to characterize textured ultrasound images of the kidney. The first texture multifractal approach is based on local information that is the singularity. Indeed, the originality of our contribution here is to use pixel singularity to build the singularity-level matrix and the binarized image(homogeneity/discontinuity), from which we extract new texture features. While the second one is based on global information provided by the multifractal spectrum. In fact, the originality of our contribution here is to use the Hausdorff multifractal spectrum that gives a better estimation of the multifractal spectrum. In this regard, to make the analysis of the spectrum possible, we had to preprocess it through smoothing, enabling us to keep the most important information of the spectrum from which we extract new texture characteristics by analyzing the shape and position of the smoothed multifractal spectrum of Hausdorff. Finally, as a second main contribution, we will evaluate the potential of our proposed multifractal features to characterize textured ultrasound images of the kidney. Having more reproducibility of the texture features first require a good choice of Choquet capacity to calculate the irregularities but also selecting a more representative region of interest (ROI) to analyze by carrying out an adapted virtual puncture in the kidney representative components.

We proceed to exclusive evaluation of the four proposed methods before evaluating the combined method of the four proposed methods and the combined one. The results of the supervised classification, using three classes of images (young, healthy, glomerulonephritis), are interesting and promising since the classification accuracy reaches about 84%. This encourages conduct further research to yield better results.

Keywords: *Multifractal Analysis, singularity, Smoothing, Hausdorff Spectrum, Texture Analysis, Kidney Image, Classification.*

ISSN: 1992-8645 www.jatit.org E-ISSN: 1817-3195

1. INTRODUCTION

1.1 Goals

The aim of the work is in first stage to propose a new multifractal approach for texture characterization by introducing new texture features extracted from singularities function and Hausdorff multifractal spectrum. Afterwards, the second goal is to perform texture characterization of kidney ultrasound image using the selected set of texture features.

1.2 Kidney ultrasound imaging

It's obvious that kidney is a vital organ that can be affected by several pathologies thus modifying its anatomical substructures and early diagnosis of them, at a preliminary stage, is a determining factor for the recovery. Indeed, ultrasound imagery is a useful, convenient and safe diagnosis modality of kidney, and the analysis of the information contained in the ultrasound image is within the competence of the clinician. Unfortunately, the quality of the ultrasound image is considered poor due to the large amount of noise, mainly speckle that is due to the interference of back scattered signals, which distorts the information sought in the image. This is why the clinician's perception must be complemented by automatic recognition based on image processing tools like texture characterization. Based on results of previous research works that reveal auto-similarity in the texture of ultrasound image, we were motivated to deepen our research on texture features from multifractal analysis [4].

1.3 Multifractal-based methods for texture characterization

Since the introduction of the fractal geometry concept[5][6] in image processing, monofractal approaches, based only on the fractal dimension that measured a degree of self-similarity at different scales, were the first to be successfully introduced for the quantification of the texture image. Indeed, as in other imaging applications [7], several proposed variants of the monofractal approach, using mathematical tools to improve fractal dimension estimation and extract new texture features, have yielded good results in medical image processing[8], and more particularly in ultrasound image analysis. For example, the differences of gray level of neighboring pixels was used by Chen and al. [9] to estimate the fractal dimension of an ultrasound image of breast lesion by using the fractal dimension. Also, local parametric fractal features extracted via maximum likelihood estimation from five well-known statistical model families are evaluated for the purpose of ultrasound liver tissue characterization [10][11]. But, due to the fractal dimension alone does not provide enough description of all regularities in the texture, the fractal dimension-based methods remain insufficient for efficient texture characterization for the real-world image.

Then fortunately several research works argued that texture characterization can be obtained by measuring the fluctuation of image amplitude regularity in space, and hence achieved by means of a multifractal analysis [12][50][51]. Indeed, with the development of the multifractal formalism [13-15], several multifractal approaches for the texture analysis has been developed using different mathematical tools namely: wavelet transform [16], capacities and measures, and methods used for calculation Hölder exponent and multifractal spectrum. Further researches were conducted leading to resolve problems where simply multifractal methods faild. For example, Kantelhardt and al. [17] proposed multifractal detrended fluctuation analysis to handle the non-stationary measures, and adapted variants of this method yielded successful results in many image processing applications [18-20]. Also, methods based on Multifractal analysis were developed for multivariate image processing [21].

All texture features extraction methods based on multifractal analysis reported in the all fields of image processing exist in two types: those based on local information given by the singularity function and others based on global information given by the multifractal spectrum.

The first one uses local information, given by the irregular singularity at each point, by building the singularity matrix from which we extract statistical and structural texture features describing the distribution of different irregularities in the whole of image. In fact, this idea has been introduced in the segmentation of textured images. Uma and al. [22] calculated of statistics on histogram of singularities to characterize synthetic aperture radar (SAR) images.

The second kind of methods uses global information given by multifractal spectrum $(f(\alpha), \alpha)$, where fractal dimension $f(\alpha)$ of different fractal components E_α have defined each one by a value of singularity α [23]. According works of Chaudhuri and Sarker [24], Xu[25] and Florindo[26], all the multifractal spectrum is considered to classify real images of texture. A

similar approach using a regional multifractal spectrum is used to analyze remote-sensing images [27]. Piotr and al.[1-3] extend this approach for texture features by showing that form and position of Legendre multifractal spectrum of texture give a valuable information on the texture image [1]. However, the criticism we make to this method is the assumption of the strong multifractal formalism. Then, we present a generalization of this method with using the Hausdorff spectrum that we pre-process before extracting features based on its shape and position. A similar approach using a regional multifractal spectrum is used to analyze remote-sensing images [27].

Finally, following our review of papers, we note that many research works reveals the potential of multifractal features to characterize human organs from ultrasound images [34]. Indeed, a promising results was yielded by research works conducted to characterize melanoma of tissue, particularly methods using wavelet Leaders like maximum wavelet coefficient [35-37]. In liver diagnosis, some works using multifractal tools were conducted to aim goals like characterizing texture of ultrasound image [38] or improved prediction of ultrasound liver tumor response to chemotherapy treatment [39]. That's in characterization of the trabecular bone microarchitecture where the good results were yielded since introduction of the monofractal model, with methods based solely on fractal dimensions [40-44], but the results have begun to be more amazing with methods based on multifractal analysis that enables a description of both local and global regularity and roughness of the trabecular bone on radiographic images [45].

1.4 Texture characterization of ultrasound kidney images

The characterization of kidney from ultrasound image was the purpose of many research works that yielded to numerous promising image processing techniques for segmentation and texture analysis. Indeed, mostly of those techniques are using texture analysis approaches based on the extraction of texture features that allow the kidney to be classified as normal or abnormal organ. These are mainly statistical texture analysis methods, based on calculating texture image statistics, such as first moment values and co-occurrence matrix for extracting local features from renal ultrasound images [28-31][54-56], but also using other texture features such as spectral statistics [32]. Wan and al [33] had developed an approach, based on the preprocessing of kidney images by Gaussian low-pass filter, with the aim to extract texture feature susing a run-length matrix in addition to second-order statistics. Generally, these research works have two disadvantages, namely that they remain unfortunately not only manual in the select of the region of interest to be studied but also with the difficulty of carrying out a complete classification taking into account different pathologies in their several stages. These disadvantages are probably the reason for the lack of papers aimed at classifying the kidney, from ultrasound images, by texture analysis based on the multifractal approach unlike the characterization of other human organs like liver or bone. This is why we attempt in our work to characterize the kidney with an adapted multifractal method based on the extraction of texture features from an ultrasound image of the kidney.

The research problem that we address in this article concerns the evaluation of the discriminative potential of new texture features, extracted from a global and local multifractal description, in a problem of characterization of kidney ultrasound images. Indeed, after an introduction of our research topic, we present, in part 2, the basic principle of multifractal analysis. Afterwards, in part 3, in order to extract new texture features from the Hölder exponent, we also present a solution that allows us to quantify the singularity by defining the level-singularity matrix. Then, new texture attributes, extracted from the global information given by the Hausdorff spectrum, are presented in part 4. Part 5 constitutes the second part of the methodology where we evaluate the discriminating power of the proposed attributes. In part 6, and within the framework of an ultrasound image characterization problem, we present the second part of the methodology in which we evaluate the discriminating power of the proposed features. Then, we finally end our article by presenting the results, the discussions, and the conclusion.

2. BASIC PRINCIPLE OF MULTIFRACTAL ANALYSIS

The fractal geometry has been introduced to describe the scale relations between geometrical structures and scale for analysis of those structures: the size of a fractal set changes as a scale from which it is examined, given by the fractal dimension [46].

The $\alpha(x, y)$, quantiying the regularity of the image in the neighborhood of the point (x, y), is defined by the singularity which is the measure of the local fractal dimension(1).

The generalization of the notion of multifractal [13] is to consider all sets of multifractal E_α as a hierarchy of sets in which, each of them has its own fractal dimension $f(\alpha)$ (2). Thus multifractal analysis gives a scale relation that requires a family of dimensions instead of one dimension as in the case of fractal geometry [47][48]. Multifractal in images analysis consists in defining measures from the gray level to calculate spectrums and to process each point based on local α and global information $f(\alpha)$.

The singularity $\alpha(x,y)$ given by the local Hölder exponent at the point (x,y) is defined by:

$$\alpha(x,y) = \lim_{dt\to 0} \frac{log\ \mu\left(B((x,y),dt)\right)}{log(dt)} \quad (1)$$

$$f(\alpha) = dim_H(E_\alpha) \quad (2)$$

Where $B\left((x,y),dt\right)$ is the ball with the center (x,y) and the radius dt, while μ is a measure.

3. IMAGE ANALYSIS BASED ON LOCAL INFORMATION

The study of the local Hölder regularity at each point of the texture image can be a mean of texture analysis because it can simply be seen as a particular combination of Hölder exponent values. This amounts to saying that a texture is made up of a set of singularities and that the value and the spatial arrangement of these singularities can provide features to characterize the texture.

Therefore, we propose a statistical and structural analysis of the singularity matrix that we will characterize by defining some amounts related to this image as:

-The statistic features relative to the arrangement of the singularity levels using the run-length matrix showing different runs of singularity levels found within the singularity level matrix.

-First-order statistics.

-The structural features calculated on the particular areas corresponding to specific values of the Hölder regularity.

3.1 The level-singularity matrix

The Hölder function calculated on an image $m \times n$ is stored in an array of the same size $m \times n$ where each point (i,j) carries the value of the Hölder exponent $\alpha(i,j)$ estimated on the pixel (i,j) (Figure 1). The realization of the image of the singularities can be carried out from a sampling of the values of singularities which consists in calculating the maximum value of the singularities α_{max} and covering the interval $[\alpha_{min}, \alpha_{max}]$ with the set of intervals I_i defined by:

$$I_i =]i\alpha_u, (i+1)\alpha_u] \quad \text{for} \quad i = 1, \dots, 14$$

with $\alpha_u = \frac{\alpha_{a,max} - \alpha_{a,min}}{16}$.

With $I_0 = [\alpha_{min}, \alpha_u]$ and $I_{15} =]15\alpha_u, \alpha_{max}]$.

α_u is the reference step defined, in a normalized way, to establish irregularity level classes within the image of the singularities. Indeed, $\alpha_{a,max}$ (resp. $\alpha_{a,min}$) the mean maximum(resp. mean minimum) calculated on N images picked up randomly from the training set.

$\alpha_{a,max} = \frac{\sum_{i=0}^{N-1} \alpha_{max}^i}{N}$ and $\alpha_{a,max} = \frac{\sum_{i=0}^{N-1} \alpha_{max}^i}{N}$

where α_{max}^i is the singularity maximum (resp. the singularity minimum) calculated on the i^{th} image of the N training images.

The Hölder image (of singularities) H is given by:

$\forall k = 1,2, \dots, m$ and $\forall l = 1,2, \dots, n$ we have:

$H(k,l) = j$ si $\alpha(k,l) \in I_j \quad \forall j = 0,1,2 \dots, 15$

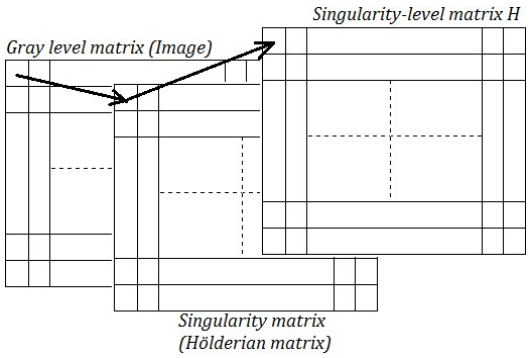

Figure 1 : The table designating the singularity level matrix calculated from the original image.

3.2 Features from run-length matrix of singularity levels

This method, using the matrix of singularity levels H containing irregularity information at each point (x,y), is based on the definition of statistical parameters expressing the distribution of the levels of singularities existing in the image. A run of irregularity-level is a consecutive set of collinear pixels having the same level of irregularity. The run-length matrix $p_\theta(i,j)$ is given counting the runs of irregularity levels i and of size j.

The run-length matrix involves two textural information, namely: the direction and the

coarseness in terms of irregularities. The direction generally used to define run-length matrix are $0^{\circ}, 45^{\circ}, 90^{\circ}, 135^{\circ}$.

The reduced number of singularity levels will make it possible to avoid the large number of runs of irregularities which contain only one point. This is how we consider the coding of singularity levels on 16 levels sufficient for texture analysis with run-length matrix.

Thus the generalized parameter defining the statistical distribution of the various runs of irregularity levels is given by:

$$GRLSLF = \frac{1}{n_\theta}\sum_{i=1}^{G}\sum_{j=1}^{N_\theta} i^{k_i} j^{k_j} p_\theta(i,j)$$

GRLSLF: Generalized Run Length Singularity Level Feature.

Where n_θ is the total number of runs existing in the singularity-level matrix H along a θ direction.

G is the number of singularity-level.

N_θ is the size of singularity-level matrix H along the θ direction.

Several texture features can be defined from the *GRLSLF* parameter by giving k_i and k_j different values. The principle in the extraction of the features is to exclusively measure the accentuation of different types of singularity-level and run-length via the coefficients k_i and k_j.We propose some feature, namely:

- Short Run Low Level Singularity Emphasis (SRLLSE) given by $k_i = -2$ and $k_j = -2$.
- Short Run High Level Singularity Emphasis (SRHLSE) given by $k_i = 2$ and $k_j = -2$.
- Long Run High Singularity Emphasis (LRHSE) given by $k_i = 2$ and $k_j = 2$.
- Long Run Low Singularity Emphasis (LRLSE) given by $k_i = -2$ and $k_j = 2$.

Other run length statistics are defined, namely:

- Run Length Non-Uniformity (*RLNU*) given by:

$$RLNU = \frac{1}{n_\theta}\sum_{j=1}^{N_\theta}\left(\sum_{i=1}^{G} p_\theta(i,j)\right)^2$$

- Singularity Level Non-Uniformity (*SLNU*) given by:

$$SLNU = \frac{1}{n_\theta}\sum_{j=1}^{G}\left(\sum_{i=1}^{N_\theta} p_\theta(i,j)\right)^2$$

- Runs Percentage (*RP*)

$$RP = \frac{1}{\sum_{i=1}^{G}\sum_{j=1}^{N_\theta} j p_\theta(i,j)}$$

3.3 First-order statistics

First-order statistics are estimated on singularity levels without taking into account their relative distribution. The consideration of these amounts calculated on the singularity level matrix allows an evaluation of the different levels of irregularities without taking into account their relative distribution in the image.

However, we will consider the most used first-order statistics, namely:

✓ The average singularity level value:

$$Av_h = \sum_{i=0}^{15} i.h(i)$$

With h the histogram of the singularity level matrix H.

This quantity makes it possible to evaluate the average irregularity-level around which the various levels of irregularities are located.

✓ Variance :

$$var_h = \frac{1}{m.n}\sum_{i=1}^{m}\sum_{j=1}^{n}\left(aver_h - H(i,j)\right)^2$$

✓ The skewness (centered space moment of order 3) :

$$\mathrm{Skew_h} = \frac{1}{\mathrm{m.n}}\sum_{\mathrm{i=1}}^{\mathrm{m}}\sum_{\mathrm{j=1}}^{\mathrm{n}}(\mathrm{H(i,j)} - \mathrm{aver_h})^3$$

✓ The Kurtosis (centered space moment of order 4) :

$$Kurt_h = \frac{1}{m.n}\sum_{i=1}^{m}\sum_{j=1}^{n}(H(i,j) - aver_h)^4$$

Other first-order statistics extracted from the singularity-level matrix H will be used like energy, entropy...

3.4 Structural features using the Hölderian matrix:

In the Hölderian matrix $\alpha(x,y)$, the points (x,y) with the low singularity value $(\alpha(x,y) << 2)$ correspond to locally irregular points including the contour points $(\alpha(x,y) \approx 1)$. While pixels with high singularity value $(\alpha(x,y) \approx 2)$ are corresponding to homogeneous regions. Consequently, the possibility of describing the two modes (discontinuity/homogeneity), in the texture, from the Hölderian matrix encourages us to

characterize it by structural features quantifying their size and distribution.

Indeed, the average singularity constitutes a texture feature which will also be used to binarize the Hölderian image by considering it as a threshold separating the two modes, namely: discontinuities and homogeneities. The Hölder regularity threshold S is the mean singularity value calculated on N images, picked up randomly from the training set, and given by:

$$S = \frac{\sum_{i=0}^{N-1} A\_S_h^i}{N}$$

Where the $A\_S_h^i$ is the average singularity value calculated on the i^{th} image with $m \times n$ size.

$$A\_S_h^i = \frac{1}{m.n} \sum_{k=1}^{m} \sum_{l=1}^{n} \alpha(k,l)$$

Therefore the binarized image H_1 is given by defining the two regions (Figure 2):

- Let R_I be the set of pixels forming the irregular regions with low singularity levels, defined by:

$$H_1(i,j) = 0 \text{ if } \alpha(i,j) \leq S$$

- Let R_H be the set of pixels forming the homogeneous regions with high singularity levels, defined by :

$$H_1(i,j) = 255 \text{ if } S < \alpha(i,j)$$

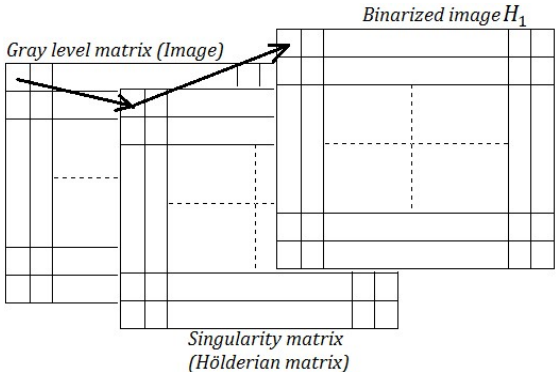

Figure 2 : The table designating the image of irregularities calculated from the Binarized image.

Our texture description, from binarized image H_1, is structural aiming to extract characteristic features describing the size and the distribution of irregular and homogenous regions.

Indeed, let $\{R_H^j\}_{j=0,..,N-1}$ the disjointed N subregions that form the partition of the homogeneous region R_H. And let Ar_H^i the area of the subregion R_H^i. Thus, the texture features we suggest are the following:

- The maximum area of homogeneity given by:

$$Ar_H^{max} = \max_i Ar_H^i$$

- The total area of homogeneity, given by:

$$Ar_H^{total} = \sum_{i=0}^{N} Ar_H^i$$

- The average area of homogeneity, given by:

$$\mathrm{Ar_H^m} = \mathrm{Ar_H^{total}} / \mathrm{N}$$

- The relative maximum area:

$$\mathrm{Ar_H^{rel,max}} = \mathrm{Ar_H^{max}} / \mathrm{A_H^{total}}$$

- The average area of homogeneity:

$$Ar_H^{m,max} = Ar_H^m / A_H^{total}$$

- The number N_H of the subregions forming the partition $\{R_H^j\}_{j=0,..,N-1}$.

We also do the same thing with the irregular subregions $\{R_I^j\}_{j=0,..,M-1}$, characterized by a low singularity values, and we extract some features, namely: Ar_I^{max}, Ar_I^{total}, Ar_I^m, $Ar_I^{rel,max}$, $Ar_I^{m,max}$, N_I.

Therefore, we can also use other structural features, like areas and positions, extracted on the Hölderian matrix (given by $\alpha(i,j)$), to describe components of the texture corresponding to different values of irregularities $\alpha(i,j)$.

4. TEXTURE ANALYSIS BASED ON MULTIFRACTAL SPECTRUM

4.1 The smoothing of the Hausdorff multifractal spectrum

Smoothing discrete curves consists of a substitution of those by regular forms from which one has good representation to access for analyzing them. The filters 1-D as median, average stage and its derivate are mostly used for smoothing functions 1-D like signal in order to eliminate noise. But the size and the number of iterations that one has to use those filters represent parameters to regulate for good results, Practically, a criteria of quality based on the distance of the curve from points (or in total quadratic error) is used to determine a regular function that realizes an optimal smoothing.

Considering n points (t_i, y_i) with $t_i \in [a,b]$, a function should, therefore, be found $f(t)$ to minimize E_1 or E_2 defined as follows:

ISSN: 1992-8645 www.jatit.org E-ISSN: 1817-3195

$$E_1 = \sum_{i=1}^{n}(f(t_i) - y_i)^2 \quad (3)$$

and $$E_2 = \max_i\{[f(t_i) - y_i]\} \quad (4)$$

Criterion of (3) and (4) make it possible to valorize results given by those two representatives' classes of filters that exist: linear filters (average) and non-linear filters (median).

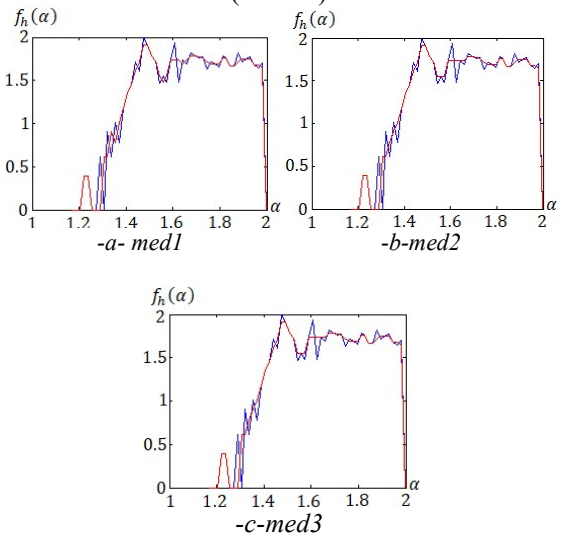

Figure 3: Smoothing of multifractal spectrum with the median filter 1D (size 1x3). a- The median filter is applied once. b- Twice. c- Three times.

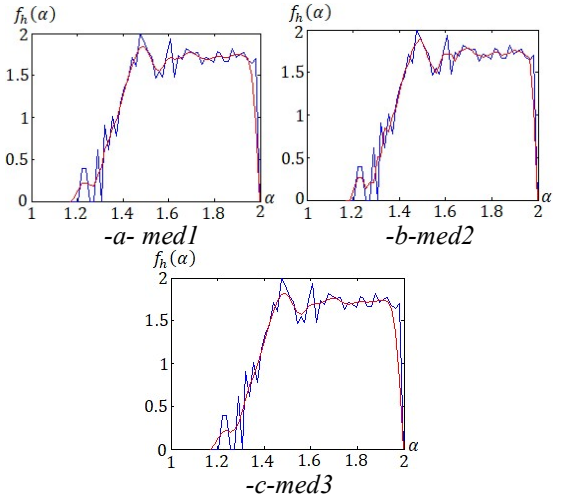

Figure 4: Smoothing of multifractal spectrum with the average filter 1D(size 1x3). a- The average filter is applied once. b-Twice. c- Three times.

We notice that the curve obtained from an average stage is smooth but the curve obtained from a median filter presents some angular points. In facts, we consider criteria (3) because it takes in consideration all points of the curve. Find results are provided in the table 1 which gives the average, the standard deviation and the coefficient of variation of quantity E_1 measured from the spectrum of a set of 40 chosen images picked up randomly.

The analysis of results proves that the average stage filter offers a regular curve form that which may be used for the texture in image analysis. Similar results had been obtained while using the criteria (4).

Table 1 : Summary of results regarding criterion (3) for a median filter and average filter.

	Median	Average
Average	0.924	0.941
Dev. Std.	0.205	0.221
Coef. Var.	22.18	34.74

The characterization of texture by analyzing the form and the position of the smoothed multifractal spectrum is now possible by using the Hausdorff multifractal spectrum which represents the most exact spectrum to estimate fractal dimension for various fractalities recovering the image.

4.2 The fractal dimension, average D_a and central D_c

The image analysis using the multifractal spectrum is at the same time easy and challenging. In fact, it is easy because the distinction of homogenous regions can be achieved by selecting sub regions of an image that has for fractal dimension a value that tends toward 2; whereas edge points are characterized by a fractal dimension neighboring 1. Otherwise it is difficult to explain sub regions with a fractal dimension different from 1 and 2, which means that the fractal set E_α that dimension is $f(\alpha) \ll 1$ or $1 \ll f(\alpha) \ll 2$. The characterization of an image by homogenous regions ($f(\alpha) \approx 2$) has a problem of limit because there is no general rule which gives the value that one has homogenous regions from the multifractal spectrum. This is why fractalities on the image have to be divided into two groups:

- All given subsets E_α defined by $f_S < f(\alpha) \leq 2$ (with $1 < \alpha_S$) having homogenous regions. This set is representative because if the texture is smooth its contribution in the multifractal spectrum becomes interesting but, it is the opposite when the texture is not smooth.
- All given subsets E_α defined by $f(\alpha) \leq f_S$ have an irregularity that corresponds to the edges. In fact, cutting the spectrum in two can be realized using an average fractal dimension defined in the same way that one defines average in physics values. In that case it is difficult to give a

signification apart from representing a statistical sampling that describes the value $f_h(\alpha)$. In our case we show how this statistic can be important in the classification of images of texture.

$$D_a = \frac{1}{M}\sum_{\alpha=\alpha_{min}}^{\alpha_{max}} f_h(\alpha) \quad (5)$$

Where M is the numer of E_α subsets.

We have two subregions that cover the image:

- The pixels (i,j) with Hölder exponent $\alpha(i,j)$ is that :

$$D_a < f_h(\alpha(i,j)) \leq 2.$$

- The pixels (i,j) with Hölder exponent $\alpha(i,j)$ is that :

$$f_h(\alpha(i,j)) \leq D_a.$$

All spectrum points given by $D_a < f_h(\alpha(i,j)) \leq 2$ belong to an interval of singularities delimited by those values:

$$\alpha_{min}^a = min\{\alpha / f_h(\alpha) = D_a\}$$

and

$$\alpha_{max}^a = max\{\alpha / f_h(\alpha) = D_a\}$$

The central Hölder exponent α_C is defined by an average of $\alpha \in [\alpha_{min}^a, \alpha_{max}^a]$. Consequently, the D_C has to be defined with respect to α_C where:

$$\alpha_C = \frac{1}{N}\sum_{\alpha=\alpha_{min}^a}^{\alpha_{max}^a} \alpha$$

Figure 5 gives different quantities of multifractal spectrum.

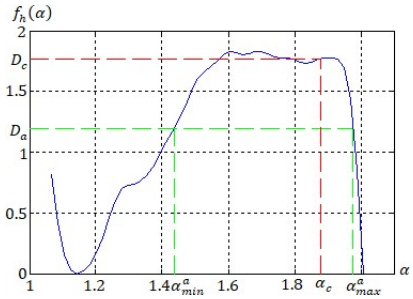

Figure 5: Example of smoothed multifractal spectrum.

4.3 Texture features

The spectrum being divided into two zones : left $\alpha < \alpha_C$ and right $\alpha \leq \alpha_C$; then one can prove that the spectrum, being with respect to those two types of irregularities, can be an element that characterizes the texture.

The position of the spectrum is defined by maximum α_{max} , minimum α_{min} and central singularities α_C, but the form can be quantified by calculating the characteristic areas of different parts of the spectrum and dispatching with respect to two axis α and $f_h(\alpha)$.

So attributs of texture are summarized here after.

4.3.1 Analysis of total spectrum

➢ Total area :

$$A_1 = \int_{\alpha_{min}}^{\alpha_C} f_h(\alpha)\, d\alpha \quad A_2 = \int_{\alpha_C}^{\alpha_{max}} f_h(\alpha) d\alpha$$

$$A_3 = {}^{A_1}/_{A_2}$$

A_1 (Respectively A_2) provides information on fractalities, defined by Hölder exponents $\alpha < \alpha_C$ (respectively $\alpha_C \leq \alpha$), based on the distribution of their dimensions. While A_3 provides information on types of fractalities with respect to the other fractal dimension.

➢ Average integral on α axis and their proportion :

$$A_4 = {}^{A_1}/_{(\alpha_C - \alpha_{min})} \quad A_5 = {}^{A_2}/_{(\alpha_{max} - \alpha_C)}$$

$$A_6 = {}^{A_4}/_{A_5}$$

A_4 (resp. A_5) provides information on the value of the dimension, which is constant on the interval $[\alpha_{min}, \alpha_C[$(resp. $[\alpha_C, \alpha_{max}]$), occupies the same area A_1(resp. A_2) of $f_h(\alpha)$ on the same interval. That value depends on the spectrum being to the support $[\alpha_{min}, \alpha_C[$ (resp. $[\alpha_C, \alpha_{max}]$). While A_6 provides information on the importance of quantities A_4 and A_5, in relation to each other.

• Percentage of total area

Given $f_{min}^l = min\{f_h(\alpha)/\alpha \in [\alpha_{min}, \alpha_C[\}$ and $f_{min}^r = min\{f_h(\alpha)/\alpha \in [\alpha_C, \alpha_{max}[\}$

$f_{max}^l = max\{f_h(\alpha)/\alpha \in [\alpha_{min}, \alpha_C[\}$ and $f_{max}^r = max\{f_h(\alpha)/\alpha \in [\alpha_C, \alpha_{max}[\}$

l : left and r : right

Then we can define those quantities:

$$A_7 = {}^{A_4}/_{(f_{max}^l - f_{min}^l)} \quad A_8 = {}^{A_5}/_{(f_{max}^r - f_{min}^r)}$$

$$A_9 = {}^{A_7}/_{A_8}$$

A_7 represents the percentage of the total area in the area of the smaller rectangle containing the left part of the spectrum. In fact, this quantity provides information on the position and the form of the spectrum on its left part because the left part

of the spectrum is higher, and the attribute A_7 shall be important. The same interpretation can be done on the right part of the spectrum. While A_9 provides information on the ratio A_7 and A_8.

4.3.2 Partial analysis of the spectrum

The spectrum has an important part where the fractal dimension has high values. We have established a method allowing us to estimate this area using the average of the dimension. Now we are going to analyses the given part of the spectrum using the Hölder exponent to the interval $[\alpha^a_{min}, \alpha^a_{max}]$ inside homogenous regions of the texture. First of all, we define similar attributes to see how the spectrum will be inside the two parts of those intervals $[\alpha^a_{min}, \alpha_C]$ and $[\alpha_C, \alpha^a_{max}]$.

So that, partial areas and derived quantities have been established.

- **Partial area :**

Given:

$$f^{l,a}_{min} = min\{f_h(\alpha)/\alpha \in [\alpha^a_{min}, \alpha_C]\}$$

and $$f^{r,a}_{min} = min\{f_h(\alpha)/\alpha \in [\alpha_C, \alpha^a_{max}]\}$$

l : left and r : right

Then we define those areas:

$$A_{10} = \int_{\alpha^a_{min}}^{\alpha_C} f_h(\alpha)d\alpha - (\alpha_C - \alpha^a_{min})f^{l,a}_{min}$$

$$A_{11} = \int_{\alpha_C}^{\alpha^a_{max}} f_h(\alpha)\, d\alpha\ - (\alpha^a_{max} - \alpha_C)f^{d,a}_{min}$$

$$A_{12} = {A_{10}}/{A_{11}}$$

A_{10} (resp. A_{11}) provides information on the form of the left part of that important region of the spectrum because this attribute gives the area of the spectrum in the nearst repair defined by singularities $[\alpha^a_{min}, \alpha_C]$ (resp.$[\alpha_C, \alpha^a_{max}]$). While A_{12} gives an idea on the importance of the ratio A_{10} and A_{11}.

- **Averages integrals on α axis and their proportion :**

Given the following values:

$$f^{l,a}_{max} = max\{f_h(\alpha)/\alpha \in [\alpha^a_{min}, \alpha_C]\}$$

and $$f^{r,a}_{min} = min\{f_h(\alpha)/\alpha \in [\alpha_C, \alpha^a_{max}]\}$$

Then given the following ratio:

$$A_{13} = {A_{10}}/{(\alpha_C - \alpha^a_{min})} \quad A_{14} = {A_{11}}/{(\alpha^a_{max} - \alpha_C)}$$

$$A_{15} = {A_{13}}/{A_{14}}$$

A_{13} (respectively A_{14}) provides information on the value of dimension, which is constant on the interval $[\alpha^a_{min}, \alpha_C[$ (resp.$[\alpha_C, \alpha^a_{max}]$), occupies the same area with A_{10} (resp. A_{11}) of $f_h(\alpha)$ on the interval $[\alpha^a_{min}, \alpha_C]$ (resp.$[\alpha_C, \alpha^a_{max}]$). This value depends on the spectrum being on its support $[\alpha_{min}, \alpha_C[$ inside the repair with the axis $\left[(\alpha^a_{min}, f^{l,m}_{min}), (\alpha_C, f^{l,a}_{min})\right)$ and $\left[(\alpha^a_{min}, f^{l,a}_{min}), (\alpha_C, f^{l,a}_{max})\right)$. This value provides information on the homogenous level of the texture which dimension is approaching and less than 2. While A_{15} provides information on the homogenous level of A_{13} and A_{14}, in relation to each other.

- **Percentage of partial area :**

$$A_{16} = {A_{13}}/{(f^{l,a}_{max} - f^{l,a}_{min})}$$

and $$A_{17} = {A_{14}}/{(f^{r,a}_{max} - f^{r,a}_{min})}$$

and $$A_{18} = {A_{16}}/{A_{17}}$$

A_{16} (resp. A_{17}) represents the percentage of the partial area A_{10}(resp. A_{11}) in the area of the smallest rectangle containing the left part (resp. right) of the central area of the spectrum. This quantity provides information on the position and the form of the spectrum inside the left part because the higher the left part if the spectrum is, the more important shall the attribute A_{16} be. While A_{18} provides the information on the ratio A_{16} and A_{17}.

5. APPLICATION FOR CHARACTERIZATION OF KIDNEY ULTRASOUND IMAGES

The system that we propose is a contribution to the automatic diagnosis of the kidney from an ultrasound image. The analysis of texture is a technique that proved reliable in the field of characterization of human organs on ultrasound images [28-39]. Indeed, we chose to evaluate our proposed multifractal approach for texture characterization by applying it to the ultrasound image of the kidney in order to characterize its physiological parameters. Indeed, the choice of the image slice and the region of interest (ROI) to study are very important given the information and the quality of different views in the ultrasound image of the kidney. This is why we choose to start by carrying out virtual punctures on the ultrasound image kidney in order to measure the texture features of the different characteristic in ROIs of the kidney.

5.1. Selecting the ROI

5.1.1. Image slice selection

The images used in this work represent the longitudinal section of the right kidney, obtained from the posterior axillary line (Figure 5). The choice of this section is based on three criteria. First, this section provides a large amount of information on the kidney and especially on the renal cortex where the nephrons (blood-filtering units) begin. Also it contains the renal medulla, which is the innermost part of the kidney, and is split up into many sections, known as the renal pyramids [53]. Finally, the frontal section allows achieving pseudo-reproducibility unlike the transverse, sagittal or oblique section.

For this characterization work of the kidney, we carried out 50 acquisitions from each of the groups, namely: healthy young people, healthy adults and pathological (glomerulonephritis cases). The acquired images are divided into two groups namely: a group for learning which contains 25 images of each class and a test group containing 25 images of each class. Note that the distribution is made randomly without preferences.

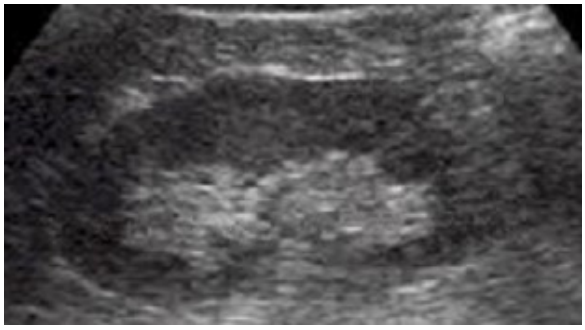

Figure 6: Ultrasound image of the frontal section of the kidney

5.1.2. Virtual ROI by selecting kidney representative regions.

The adoption of a multifractal approach for the characterization of the texture of an ultrasound image of the kidney poses the problem of the choice of a representative region in which the local singularities and the multifractal spectrum should be calculated. We, therefore, opted for a virtual puncture in which the representative region of interest (ROI) would be a rectangular window of size mxn selected over the region of interest to be studied.

Indeed, selecting the ROI on the longitudinal section is the best choice because it clearly shows the two main components of the kidney, namely: the parenchyma which consists mainly of the cortex and the medulla, and the central zone consisting of the calyces, sinuses and pelvis.

This is why we aim in our work to measure the informational contribution of these two main components by initially selecting the ROI only on the parenchyma (Figure 7.a) to evaluate the state of the kidney based on the image texture consisting of the cortex and the pyramids. This window size is about 50x120 pixels and is selected as much as possible in the horizontal part of the component consisting of the cortex and the medulla.

The second ROI we selected is a window with a size of 50x120, centered as much as possible, on the central area (Figure 7.b) to evaluate the state of the kidney based on the image texture consisting of the calyces, sinus and pelvis.

Finally, we selected another ROI considering both components at the same time(Figure 7.c). This « representative » region of the entire kidney is about 80x180 pixel window and includes both components as much as possible. (Figure 6). The size of the selected window depends solely on the size of the kidney.

The only limitation is that the selection of the ROIs is done manually, and in a few cases we are unable to select a region of interest with the defined size, which is also the case for small kidneys. This is also the case for certain cases of young subjects and certain pathological kidneys whose size decreases in the advanced stages of the pathology.

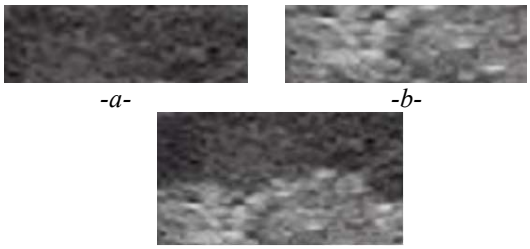

-a- *-b-*

-c-

Figure 7*: a- The representative window of the renal parenchyma area (cortex and medulla). b- The representative window of the central area (pelvis, calyxes and sinus). c- The window representative of the kidney containing part of the two regions.*

5.2 Choice of analysis capacity

We recall that the right framework for image processing via a multifractal approach is that of capacities. The class of capacities usually used in image processing is that of Choquet capacities.

Indeed, all the results and methods resulting from the multifractal analysis of the measurements remain valid for the multifractal analysis of the capacities of Choquet which can be extended to the multifractal analysis of the images. Multifractal analysis of Choquet capacities is widely described in [13].

We define on a region A, according to the resolution n, the most used Choquet capacities:

$$C^n_{max}(A) = max\{L(x^n_{k,l})/x^n_{k,l} \in A\}$$

$$C^n_{sum}(A) = \left\{ \left(\sum_{x^k_{n,l} \in A} \left(L(x^n_{k,l})\right)^p \right)^{1/p} \right\}$$

$$C^n_{iso}(A) = max\, card\{(k,l)/L(x^n_{k,l}) = t \;\; with \;\; x^n_{k,l} \in A\}$$

Where L is the gray level function.

The properties of these capacities are:

✓ $C^n_{max}(A)$ depends only on the value of the gray levels.

✓ $C^n_{sum}(A)$ depends on the gray levels of the pixels of region A and their distribution.

✓ $C^n_{iso}(A)$ depends only on the distribution of gray levels.

Indeed, each capacity reveals a different aspect of the image, which is why the choice of the capacity depends extremely on the application and the information that one aims to extract from the image. There is no general method to choose one that is optimal for a given problem because this choice takes into account several criteria:

✓ Simplicity and speed of calculations.
✓ Robustness to noise.
✓ Relevance regarding the type of images.

Table 2: Statistics of parameters α_{min},α_{max} and α_C calculated with Choquet capacities (a)maximum, (b)sum, (c)iso.

	Parenchymal region			Central region		
	α_{min}	α_{max}	α_c	α_{min}	α_{max}	α_c
Mean	0.005	0.585	0.064	0.006	0.452	0.091
Std. Dev.	0.001	0.175	0.020	0.000	0.074	0.020
Coef.Var.%	28.81	30.05	32.35	10.93	16.43	22.40

-a-

	Parenchymal region			Central region		
	α_{min}	α_{max}	α_c	α_{min}	α_{max}	α_c
Mean	1.869	2.379	1.977	1.891	2.235	1.991
Std. Dev.	0.017	0.176	0.009	0.068	0.055	0.008
Coef.Var.%	0.94	7.41	0.47	3.59	2.47	0.42

-b-

	Parenchymal region			Central region		
	α_{min}	α_{max}	α_c	α_{min}	α_{max}	α_c
Mean	1.173	1.9763	1.8244	1.3111	1.9869	1.8735
Std. Dev.	0.057	0.010	0.034	0.088	0.004	0.022
Coef. Var. %	4.88	0.52	1.89	6.71	0.22	1.19

-c-

The choice of capacity cannot be made without evaluating the stability of the results obtained with each capacity. This evaluation consists of the measurement of the stability of the particular values characterizing the multifractal spectrum by the shape and the position [1] namely: the minimum and maximum singularities (α_{min} and α_{max}) and the central singularity α_C which corresponds to the average fractal dimension (see table 2).

Indeed, we proceeded with the calculation of the Hausdorff spectrum on a set of images belonging to the class of healthy adult subjects as a reference. The apparent difference in echogenicity enables us to distinguish the two regions of interest, parenchyma and central region, on each image. Then, we calculate the Hausdorff spectrum on each of the two regions. In the tables (Table 2), where we give the results relating to the various measurements carried out on 15 images, we notice a significant variability of the parameters α_{min}, α_{max} and α_C, by using the max capacity, whereas it is low for the sum and iso capacities. This finding excludes the max capacity.

Therefore, we choose the iso capacity because it is insensitive to the image dynamics which can change from one subject to another.

5.3 Texture features extraction

As previously described, the extraction of our multifractal texture feature will be performed on selected windows representative of the parenchyma, central, and boundary region between them and containing part of both components at the same time. It is recalled that the features extracted are quantities with which the shape and position of the Hausdorff multifractal spectrum have been quantified, as well as statistical and structural quantities calculated on the image of the singularities.

- ***Texture features based on local information***

As described in 3, to perform a local multifractal description of the ultrasound images of the kidney, we will use texture features calculated from the singularity level matrix of the three selected regions of interest, namely: parenchyma, central and representative region of the "whole" kidney. The first part of these features, given in 3.2 and 3.3, are respectively the statistics extracted from the singularity-level run-length matrix and the first-order statistics extracted from the Hölderian matrix. While the second part of the features, given

in 3.4, are the structural features that we extract from the binarized image (Figure 9) carried out from of the Hölderian matrix.

On figure 8, we give the images corresponding to the singularity-level matrix of the three regions of interest representative of regions namely: the parenchyma, the central and the "whole" of the kidney.

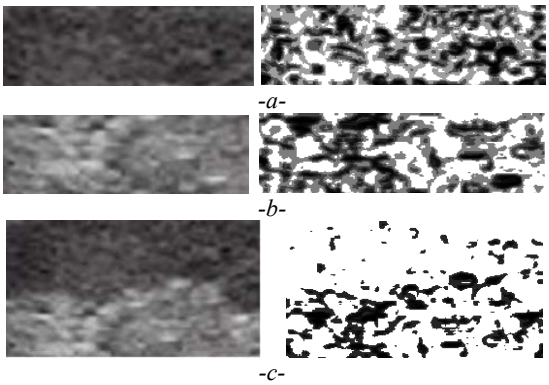

Figure 8: The ROI of the considered region of the kidney on the left and its image of the singularity levels on the right. (-a-: the parenchyma, -b-: the central, -c-: the "whole" kidney)

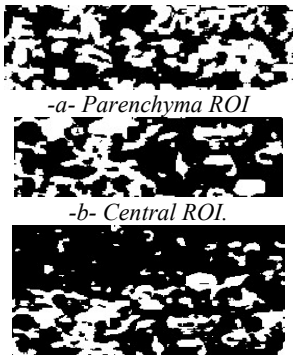

Figure 9: Binarized images showing the two irregularities modes: discontinuous regions in black and homogeneous regions in white.

- ***Texture features based on the multifractal spectrum:***

As described in 4, to perform a global multifractal description of the ultrasound images of the kidney, we will use texture features calculated on the Hausdorff multifractal spectrum of the three selected regions of interest. Indeed, as we have shown previously, we propose in our procedure to smooth the Hausdorff spectrum by a mean filter given in 4.1, before extracting the features.

Here, in figure 10 we present the results relating to the different smoothing methods by giving in each graph (a, b and c) the spectrum of each of the three regions analyzed, namely: the parenchyma, the central and the region representing the "whole" kidney.

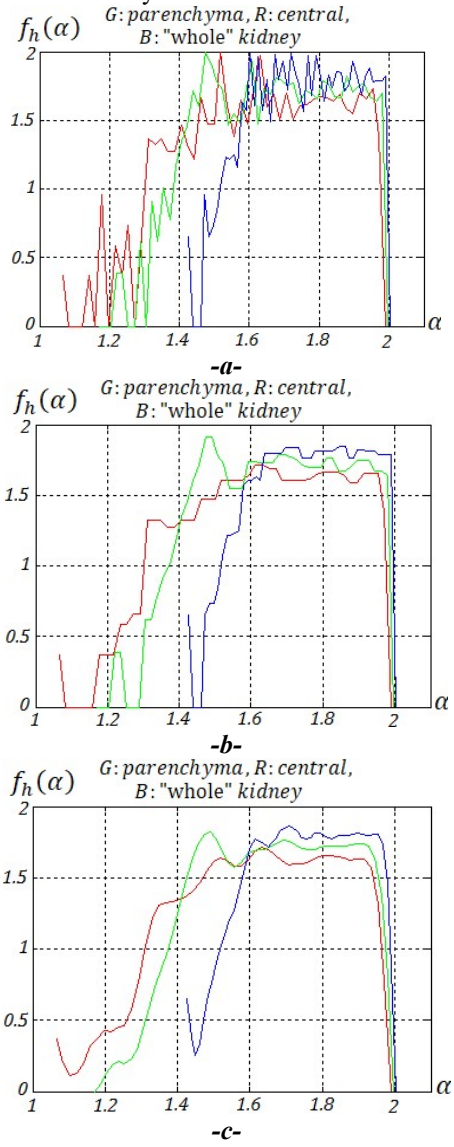

Figure 10: -a- The multifractal spectrum calculated on the three ROIs. -b- Spectrum smoothed with the median filter. -c- Spectrum smoothed using the mean filter.

Then, the features $(D_\alpha, D_C, D_m, A_1, A_2, \ldots, A_{18})$, that are given in 4.2 and 4.3, are extracted from the smoothed Hausdorff multifractal spectrum.

6. RESULTS AND DISCUSSIONS

In this paragraph, we aim to evaluate the discriminating power of our texture analysis approach by choosing the most discriminating features through an iterative bottom-up selection procedure[53]. Indeed, with a supervised classification method, two goals are targeted at the same time, namely: the selection of all the most representative features and the evaluation of the discriminating power of the approach which will be given by the correct classification rate obtained by the selected subset of features. Indeed, the classification is carried out on a test set, knowing that we have a learning set with which we define the different classes beforehand.

In this sense, the classification method used is that of the K-Nearest Neighbors (KNN) which is a reliable and easy to implement method.

Before carrying out the evaluation of the classification accuracy of the combined method, we first conduct an exclusive evaluation of the classification accuracy of each of the proposed methods, namely: singularity level run-length matrix, first order statistics, structural features and the multifractal spectrum features.

Then, we considering the representative window of each of the three ROIs (parenchyma, central and "whole" kidney) on which we proceed as the following:

- By analyzing the evolution of the classification accuracy according to the number of features used, we obtain the best result with a subset of features which allows the best classification accuracy. Indeed, we proceed by using the images of the training set and the processing was carried out for three values of the parameter K=6,7,8.
- We also calculated the influence ΔT_c of the parameter K (K=6,7,8) by measuring the mean, on all the iterative process, of the variation of the classification accuracy.
- Using the images of the test set and performing the classification with the features that give the best classification accuracy rate, we obtain the confusion matrix which is a summary of prediction results on our classification problem. Also we can find in the confusion matrix more detailed information about the distribution of misclassified and well-classified images.

6.1. The parenchyma region of interest

The results obtained, by considering the representative window of the parenchyma, are noted in table 3. Indeed, analyzing the results allow us to make the following remarks:

- Both methods, singularity level run-length matrix and the structural description, clearly provide the best classification accuracy rates.
- The impact of the choice of the number K (K=6,7,8) remain not significant with ΔT_c less than 7.3%.
- The best result is obtained using the combined method. Indeed, the best classification accuracy rate reachs about 75.8%, and obtained with 14 features.
- The number of the features obtained with the combined method shows that there is a correlation between the features, and in particular between the most discriminating features selected during the exclusive use of each of the four method.

Table 3 : Classification accuracy results with the K-nn method (K=6,7,8). (NTF: The number of texture features)

	K=6	K=7	K=8	ΔT_c	NTF
Singularity level Run-length matrix	71.2%	70.5%	69.1%	5.3%	6
First order statistics	50.4%	51.0%	49.6%	6.5%	3
Structural features	68.5%	67.1%	65.7%	7.3%	4
Multifractal spectrum	63.5%	65.2%	65.8%	4.1%	9
Combined method	75.8%	76.1%	74.9%	5.7%	14

Table 4: The confusion matrix giving the result of the test classification.

Expected class	Predicted class			
		Young	Healthy	Patho.
	Young	19	6	0
	Healthy	8	16	1
	Glomerul	2	2	21

The results of the set test classification are summarized in the confusion matrix (Table 4). Indeed, the analysis of the results allows us to make the following remarks:

- The test classification accuracy rate is about 74.6%.
- The most important confusion is between healthy and young classes. This confusion is certainly due to the state of the kidney which does not show a great difference for the two

classes, particularly for our chosen young subjects that are between 14 and 18 years old.

6.2. The region of interest in the central region

The results obtained, by considering the representative window of the central region, are noted in (Table 5).

Indeed, analyzing the results allow us to make the following remarks:

- The classification accuracy rates of the four methods are weak. Even using the combined method, the results remain insignificant with a best classification accuracy rate reaching about 59.8% obtained with 11 texture features.
- Both methods, singularity level run-length matrix and the multifractal spectrum, provide slightly better classification accuracy rates.
- The impact of the choice of the number K(K=6,7,8) remain not significant with ΔT_c less than 5.5%.

The results of the set test classification are summarized in the confusion matrix(Table 6). Indeed, the analysis of the results allows us to make the following remarks:

- The test classification accuracy rate is about 54.6%.
- The confusion is quite significant between the three classes. This confusion is certainly due to the state the central region (calyces, sinuses and pelvis), which may not be affected by the pathology that is the glomerulonephritis (stage 1).

Table 5 : Classification accuracy results with the K-nn method (K=6,7,8). (NTF: The number of texture features)

	K=6	K=7	K=8	ΔT_c	NTF
Singularity level Run-length matrix	59.3%	54.2%	58.1%	2.9%	3
First order statistics	37.3%	38%	34.2%	5.6%	2
Structural features	42.5%	54.7%	41.6%	3.2%	3
Multifractal spectrum	51.3%	53.8%	52.4%	4.5%	5
Combined method	59.3%	59.8%	57.5%	5.5%	11

Table 6: The confusion matrix giving the result of the test classification.

Expected Class	Predicted Class			
		Young	Healthy	Glomerul
	Young	14	8	5
	Healthy	8	11	6
	Glomerul	4	6	16

6.3. The region of interest is the representative window of the "whole" kidney:

The results obtained, by considering the representative window of the "whole" kidney, are noted in table 7. Indeed, analyzing the results allow us to make the following remarks:

- All the methods, except the fist-order statistics, provide balanced classification accuracy rates with slight superiority for the structural description.
- The best result is obtained using the combined method. Indeed, the best classification accuracy rate reachs about 84.6%, and obtained with 16 features.
- The quite high impact of the choice of the parameter K (ΔT_c reachs 12.2%) over the results can be explained by the inhomogeneity of the texture. Indeed, the window representative of the "whole" kidney contains both a part of the parenchymal region and of the central region, which are clearly different in terms of echogenicity, in particular for healthy and young subjects.
- The number of the features obtained with the combined method shows that there is a correlation between the features, and particular between the most discriminating features selected during the exclusive use of each of the four method.

Table 7 : Classification accuracy results with the K-nn method (K=6,7,8). (NTF: The number of texture features)

	K=6	K=7	K=8	ΔT_c	NTF
Singularity level Run-length matrix	77.1%	73.2%	75.8%	9.1%	6
First order statistics	64.5%	73.9%	72.4%	9.4%	4
Structural features	79.5%	77.4%	78.3%	8.2%	7
Multifractal spectrum	75.5%	71.8%	75.6%	12.2%	9
Combined method	84.6%	78.7%	82.7%	10.7%	16

The results of the set test classification are summarized in the confusion matrix(Table 8). Indeed, the analysis of the results allows us to make the following results:

- The test classification accuracy rate is about 84%.
- The most important confusion is between healthy and young classes. The interesting thing is that the best classification accuracy is obtained with the pathological class.
- The high discriminating power of the features extracted from the multifractal spectrum justifies their power to characterize the inhomogeneity existing in the texture image representative of the "whole" kidney.

Table 8: The Confusion Matrix Giving The Result Of The Test Classification.

		Predicted class		
		Young	Healthy	Glomeru
Expected class	Young	21	4	1
	Healthy	5	19	1
	Glomerul	0	2	23

It should be highlighted that this research work forms a contribution to the design of a renal diagnostic aid system using texture analysis of kidney ultrasound images. Indeed, the results of this contribution can be improved by a more adequate pre-processing and an optimal choice of the region of interest. Moreover, the proposed new texture features, which we extracted from the multifractal description, can be used in other image processing applications.

7. CONCLUSION

Finally, we emphasize that it is very difficult to compare our results with others for three main reasons:

- The challenge of realizing a renal diagnostic decision support systems, using texture characterization of the ultrasound image, has always been presented as a semi-automatic problem, and in a non-standardized manner. This is due to the textural inhomogeniety of the ultrasound image of the kidney whose anatomy can be seen as made up of two sub-regions, namely: the parenchyma and the sinus. Therefore, the fixed purposes and the used region of interest for processing are not always the same.
- Following our in-depth review of research articles on this topic, we conclude that they are differentiated by the choice of classes, corresponding to the different pathologies of the kidney, in the supervised classification. Among the values assigned to the number of classes p taken into account, defined a priori, within the representation space, we find:
  - p=2 : normal or disead kidney[31]. Normal and cystics[29].
  - p=3 : Medical renal disease and cyst[28]. Three Chronic Kidney Diseases(CKD) stages 1, 2 and 3 [30]. Normal, glomerulonephritis, or pyelonephritis[32]. Norma, mild and moderate CKD, and severe CKD[56].
  - p=4 : Normal, cyst, renal failure and angiomiolipoma[55].
  - p=5 : Normal, cyst, stone, tumor, and failure[54].

By comparing the informational contribution of the parenchyma and the central region, we find that that of the parenchyma is even more interesting. While the "whole" kidney region, containing both part of the parenchymal and part of the central, gives a relatively better classification accuracy. It appears like that the informational contribution of parenchyma is the most predominant in that contained in the representative window of the "whole" kidney where the highest discriminating power obtained reaches about 84%, which shows slight complementarity of the texture characterization between the parenchyma and central regions.

The explanation is that glomerulonephritis is the only renal pathology considered in our study that is mainly due to a failure in the glomeruli that localize mainly in the parenchyma. Indeed, the good vitality of the glomeruli in young healthy subjects and the less good vitality in healthy adults are responsible for the low confusion which exists between these two groups, whereas the distinction of the pathological group is remarkable. It is very important to conclude already that the size of the database and the type of pathology it contains are determining factors.

We have not placed much importance on the features selection because there is a risk of excluding features that probably have a discriminating power in the classification of images belonging to a larger database. And conversely, others with little or no discriminating power in this classification can be so by considering other types of pathologies.

ISSN: 1992-8645 www.jatit.org E-ISSN: 1817-3195

The results obtained using the proposed approach are interesting and promising for the realization of a diagnostic aid system for ultrasound images of the kidney. However, the perspectives of our work will take into account several points, some of which constitute the limitations of our contribution, namely:

✓ The increase in the size of the database so that it contains other classes of images corresponding to different pathologies while carrying out image acquisitions in the most standard conditions.

✓ Proposing to use texture features that can be more effective for the characterization of ultrasound images.

✓ Setting the parameters that most influence the reproducibility of the texture features.

✓ Combining the multifractal approach with other texture characterization approach to improve the results.

✓ We encourage to applying this approach for the characterization of texture images of other human organs such as the liver.

✓ Improving a selecting puncture using a segmentation for considering all the kidney images.

REFERENCES:

[1] P. Stanszyk, P. Sharpe. "Classification of Natural Images from Shape Analysis of the Legendre Multifractal Spectrum," in Dekking et al, Fractals: Theory and Applications in Engineering, Springer- Verlag, London,1999, pp. 67-79. DOI: 10.1007/978-1-4471-0873-3_5

[2] Mohamed Abadi and Enguerran Grandchamp. "Legendre spectrum for texture classification," 8th International Conference on Signal Processing (ICSP). 16-20 November 2006. DOI:10.1109/ICOSP.2006.345588

[3] M.P. Paskas, B.D. Reljin, I.S. Reljin. "Revision of multifractal descriptors for texture classification based on mathematical morphology". Pattern Recognition Letters 83(1), 2016, pp. 75-84. DOI :10.1007/s11263-009-0220-6

[5] Pentland A. "Fractal-based description of natural scenes". IEEE Trans Pattern Anal Mach Intell;6(6), 1984, pp661 –674.

[6] Fortin C, Kumaresan R, Ohley W, Hoefer S. "Fractal dimension in the analysis of medical images." IEEE Eng Med Biol;11(2), 1992, pp 65 – 71.

[7] S.W. Myint,. "Fractal approaches in texture analysis and classification of remotely sensed data : comparaisons with spatial autocorrelation techniques and simple descriptive statistics." Int J. Remote Sensing 24, 2003, pp. 1925-1947. DOI:10.1080/01431160210155992.

[8] I. Gosciniak, K.Gdawiec, K.Wozniak, M.Machoy. "An approach to determine the features of Dental X-ray images based on the fractal dimension". Procedia Computer Science 192, 2021, pp.1856-1865. DOI:10.1016/j.procs.2021.08.191

[9] D-R Chen, R-F Chang, C-J Chen, M-F Ho, S-J Kuo, S-T Chen, S-J Hung, W K Moon. "Classification of breast ultrasound images using fractal feature." Journal of Clinical Imaging 29, 2005, pp.235-245.

[10] O.S. Al-Kadi, D.Chung, C.C.Coussios, J.A. Noble. "Hetergeneous Tissue Characterization Using Ultrasound: A Comparaison of Fractal Analysis Backscatter Models on Liver Tumors." Ultrasound in Medicine & Biology 42(7). 2016, pp.1612-1626. DOI:10.1016/j.ultrasmedbio.2016.02.007

[11] O.S.AL-Kadi, D.Y.F. Chung, R.C. Carlisle, C.C. Coussios, J. Alison Noble. "Quantification of Ultrasonic Texture Intra-Heterogenity Via Volumetric Stochastic Modeling for Tissue Characterization." Medical Image Analysis, volume 21, issue 1, 2014, pp.59-71. DOI : 10.1016/j.media.2014.12.004

[12] H.Went, S.Jaffard, P.Aubry, H.Ji." Wavelet Leader Mulrifractal Analysis for Texture Classification." Proceedings of the International Conference on Image Processing, ICIP 2009, 7-10 November 2009, Cairo, Egypt. DOI:10.1109/ICIP.2009.5414273

[13] J. Levy Vehel, R. Vojak, "Multifractal analysis of Choquet Capacities :preliminary results, " rapport de recherche de INRIA, RR-2576, Juin 1995.

[14] J. P. Berrior. "Analyse Multifractale d'Images. " Thèse de doctorat de l'Université Paris IX.Paris, France, 1994.

[15] J. Levy Vehel, P. Mignot, and J.-P. Berroir. "Texture and multifractals: New tools for image analysis." Technical Report 1706, Institut National de Recherche en Informatique et en Automatique, 1992.

[16] S.Wang, G.Wang, 2017. "Texture Classification by Multifractal Spectrum and Barycentric Coordinates of bit Planes of Wavelet Coefficients." Image Processing, IET 11(12), 2017, pp.1205-1209. DOI:10.1049/iet-ipr.2016.0875

ISSN: 1992-8645 www.jatit.org E-ISSN: 1817-3195

[17] J.W. Kantelhardt, S.A. Zschiegner, E.Koscienlny-Bunde, S.Halvin, A.Bunde, H.E.Stanley. "Multifractal Detrended Fluctuation Analysis of Nonstationary Time Series." Physica A 316, 2002, pp.87-114. DOI : 10.1016/S0378-4371(02)01383-3

[18] M.T.Castellanos, M.C.Moratos, P.L.Aguado, J.P. del Monte, A.M. Tarquisj. "Detrended Fluctuation Analysis for Spatial Characterisation of Landscapes." Biosystems Engineering 168, 2018, pp.14-25. DOI : 10.1016/j.biosystemseng.2017.09.016

[19] F.Wang, D-L Liao, J-W.Li, g-p Liao. "Two-dimensional Multifractal Detrended Fluctuation Analysis for Plant Identification." Plant Methods 11(1), 2015, pp.1-11. DOI:10.1186/s13007-015-0049-7

[20] F.Wang, Z-S.Li, J-W.Li. "Local Multifractal detrended fluctuation analysis for non-stationary Image's Texture Segmentation." Applied Surface Science 322, 2014, pp.116-125.

[21] H.Wendt, S.Combrexelle, Y.Altmann, J-Y. Tourneret, S.Mclaughlin, P.Abry. "Multifractal Analysis of Multivariate Images Using Gamma Markov Random Field." SIAM Journal on Image Sciences11(2). 2018, pp.1294-1316. DOI:10.1137/17M1151304

[22] U. S. Ranjan and A. Narayana, "Classification Of Objects In SAR Images Using Scaling Feature", ICVGIP, December 16-18, Space Applications Centre Ahmedaba, 2002.

[23] Saucier, A., Richer, J. and J.Muller, "Assessing the scope of the multifractal approach to textural characterization with statistical reconstruction of images." Physica, vol.A 311, 2002, p.231-259. DOI : /10.1016/S0378-4371(02)00814-2

[24] B.B. Chaudhuri and N. Sarkar, "Texturesegmentation using fractal dimension", IEEE. Trans. On Pattern Analysis and Machine Intelligence, Vol. 17, No. 1, 1995, pp. 72-77. DOI: 10.1109/34.368149

[25] Y.Xu, C. Femüller. "Viewpoint Invariant Texture Description Using Fractal Analysis," International Journal of Computer Vision volume 83, 2009, pp.85–100. DOI:10.1007/s11263-009-0220-6

[26] J.B. Florindo, O. M. Bruno, G. Landini. Multifractal Texture Analysis using a Dilation-based Hölder Exponent. In Proceeding of the 10th International Conference on Computer Vision Theory and Applications(VISAPP-2015), 2015,pp.505-511. DOI:10.5220/0005302305050511.

[27] P. Sailhac, F. Seyler, "Texture characterization of ERS-1 images by regional multifractal analysis," Springer-Verlag. 1997, pp. 32-41. DOI : 10.1007/978-1-4471-0995-2_3

[28] K.Sharma, J.Virmani. "Haralick's Texture Descriptors for Classification of Renal Ultrasound mages." Hybrid Intelligent Techniques for Pattern Analysis and Understanding, 2017, pp.277-310.DOI:10.1201/9781315154152-12

[29] P. T. Akkasaligar, S. Biradar, 2014. "Classification of Ultrasound Images of Kidney." IJCA Proceedings on International Conference on Information and Communication Technologies (ICICT-2014), 2014, pp.24-28.

[30] R.Ahmed, B.K.Mohanty. "Chronic Kidney Disease Stage Identification Using Texture Analysis of Ultrasound Images." Biomedical Signal Processing and Control 69 : 102695, 2021. DOI : 10.1016/j.bspc.2021.102695

[31] F.Iqbal, A.S.Pallewatte, J.P.Wansapura. "Texture Analysis of Ultrasound Images of Chronic Kidney Disease." Seventeenth International Conference on Advances in ICT for Emerging Regions (ICTer), Colombo, Srilanka, 2017 pp.299-303.DOI:10.1109/ICTER.2017.8257787

[32] M.Garelnabi, I.Abdullah, A.H.A. Bakry, E.A.Abdulla, M.Adam, 2016. "Characterization of Kidney Infection in Ultrasound B-mode Images Using Texture Analysis." International Journal of Science and Research 5(8) ISSN(Online) :2319-7064, 2016. DOI:10.21275/ART20161121

[33] W.N.H.Wan Kairuddin, W.M.h.Wan Mahmud. "Texture Feature Analysis for Different Resolution Level of Kidney Ultrasound Images." International Research and Innovation Summit (IRIS2017) 6–7 May 2017, Melaka, Malaysia, IOP Conference Series: Materials Science and Engineering, Volume 226(1), 012136, 2017.
DOI:10.1088/1757-899X/226/1/012136

[34] A. Ouahabi, S. Femmam. "Wavelet-based multifractal analysis of 1-D and 2-D signals: New results. " Analog Integrated Circuits and Signal Processing 69(1), 2011, pp.5-13. DOI:10.1007/s10470-011-9620-y

ISSN: 1992-8645 www.jatit.org E-ISSN: 1817-3195

[35] E. Villain, H. Wendt, A. Basarab, D. Kouamé. "On multifractal Tissue Characterization in Ultrasound Imaging." 16th IEEE International Symposium on Biomedical Imaging (ISBI 2019), Venice, Italy. 2019, pp.1708-1712. DOI : 10.1109/ISBI.2019.8759404

[36] A.Ouahabi. "Multifractal Analysis for Texture characterization : A New Approach Based on DWT." 10th International Conference on Information Sciences, Signal Processing and their Applications, ISSPA 2010, Kuala Lumpur, Malaysia, 10-13 May, 2010, pp. 698-703. DOI:10.1109/ISSPA.2010.5605576

[37] M.Djeddi, A.Ouahabi, H.Batatia, A.Basarab, D. Kouamé. "Discrete wavelet for multifractal texture classification: application to medical ultrasound imaging." Proceedings of 2010 IEEE 17th ICIP, september 26-29. 2010, pp.637-640. DOI : 10.1109/ICIP.2010.5650017

[38] S.S. Xu, C.Chang, C.Su, P.Q.Phu. "Classification of Liver Diseases Based on Ultrasound Image Texture Features." Applied Sciences 9(2), 2019, pp.342-367. DOI : 10.3390/app9020342

[39] O.S.AL-Kadi, D.V. De Ville, A. Depeursing. "Multidimensional Texture Analysis for Improved Prediction of Ultrasound Liver Tumor Response to Chemotherapy Treatment." Medical Image Computing and Computer-Assisted Intervention – MICCAI 2016, pp.619-626. DOI : 10.1007/978-3-319-46720-7_72

[40] Fabio Baselice, "Ultrasound image despeckling based on statistical similarity," Ultrasound Med. Biol. (2017) 2065 43.9, DOI:10.1016/j.ultrasmedbio.2017. 05.006.

[41] E.A. Abdulhameed, N.H. Al-Rawi, A.T. Uthman, A.R.Samsudin. "Bone Texture Fractal Dimension Analysis of Ultrasound-Treated Bone around Implant Site : A Double-Blind Clinical Trial." International Journal of Dentistry, 2018(1), 2018, pp.1-10, DOI: 10.1155/2018/2672659

[42] G. Bianciardi, S. Bisogno, I. Bertoldi, L.Laurini, G. Coviello, B.Frediani. "Fractal dimension of bone texture in radiographs correlates to ultrasound broadband attenuation T-score." Clinical and Experimental Rheumatology 31(1), 2013, pp.398-393.

[43] J. Velazquez-Ameijide, S.Garcia-Vilana, D.Sanchez-Molina, J.Matinez-Gonzalez. "Prediction of Mechanical properties of human rib cortical bone using fractal dimension." Computer Methods in Biomechanics Biomedical Engineering 24(5), 2020, pp.506-516.DOI: 10.1080/10255842.2020.1836623

[44] J.Y Rho, D.Flaitz, V.Swarnakar, R.S.Acharya. "The Characterization of Broadband Ultrasound Attenuation and Fractal Analysis by Biomechanical Properties." Bone (ScienceDirect), 20 (5), 1997, pp.497–504. DOI: 10.1016/s8756-3282(97)00022-7

[45] O.Bouzeboudja, B.Haddad, A.Taleb-Ahmed, S.Ameur, M.El Hassouni, R.Jennane. "Multifractal Analysis for Improved Osteoporosis Classification." Biomedical Signal Processing and Control 80, 104225, 2023. DOI:10.1016/j.bspc.2022.104225

[46] B.B. Mandelbrot, "Fractal Geometry of Nature.", San Francisco, CA Freeman 1982. DOI :10.1002/esp.3290080415

[47] A. Pentland "Fractal Based Description of Natural Scenes." IEEE Transactions on Pattern Analysis and Machine Intelligence, Vol. PAMI-6, 1984, pp. 661-674. DOI: 10.1109/TPAMI.1984.4767591

[48] LM Kaplan. "Extended Fractal Analysis for Texture Classification and Segmentation." IEEE Transaction on Image Processing, Vol.8, No. 11, 1999, pp. 1572-1585. DOI: 10.1109/83.799885

[49] O.Bouzeboudja, B.Haddad, A.Taleb-Ahmed, S. Ameur, M. El Hassouni, R. Jennane. "Multifractal Analysis FOR Improved Ospeoporosis Classification." Biomedical Signal Processing and Control 80(1), 2023. DOI : 10.1016/j.bspc.2022.104225

[50] R.Lopes, N.Betrouni. "Fractal and Multifractal Analysis : A Review." Medical Image Analysis 13, 2009, pp.634-649. DOI: 10.1016/j.media.2009.05.003

[51] R.Lopes, P. Dubois, I.Bhouri, M.H.Maouche, N.Betrouni. "Local Fractal and Multifractal Features for Volumic Texture Characterization." Pattern Recognition 44, 2011, pp. 1690-1697. DOI : 10.1016/j.patcog.2011.02.017

[52] F.S. Well, "Précis d'échographie Digestive et Rénale : Deuxième partie Echographie Rénale, " 1991. Editions VIGOT.

[53] R. Muzzolini, "A Volumetric Approach to Segmentation and Texture Characterisation of Ultrasound Images, " Thèse de PHD en Informatique, université de Saskatchewan, 01 Avril 1997.

ISSN: 1992-8645 www.jatit.org E-ISSN: 1817-3195

[54] M. W. Attia, H. E. Moustafa, F.E.Z. Abou-Chadi, N. Mekkey. "Classification of Ultrasound Kidney Images Using PCA and Neural Networks." International Journal of Advanced Computer Science and Applications(IJACSA), vol. 6, No. 4, 2015. DOI : 10.14569/IJACSA.2015.060407

[55] N. Soumya, PP. Narayanan. "Classification of Kidney Disorders From Ultrasound Images Using Adaptive Neuro-Fuzzy Inference System." International Journal of Scientific Engineering and Applied Science (IJSEAS), Vol. 1, Issue 3, May 2015. DOI : 10.14569/IJACSA.2015.060407

[56] D.-H. Kim and S.-Y. Ye, "Classification of chronic kidney disease in sonography using the GLCM and artificial neural network," Diagnostics journal (MDPI), vol. 11, no. 5, 2021, pp. 864-980.